

## Thermal Control of the Intrinsic Magnetic Damping in a Ferromagnetic Metal

José Holanda<sup>1,\*</sup>, O. Alves Santos<sup>2</sup>, and Sergio M. Rezende<sup>3</sup>

<sup>1</sup>*Departamento de Física, Universidade Federal do Espírito Santo, 29075-910, Vitória, ES, Brazil*

<sup>2</sup>*Physics of Nanodevices, Zernike Institute for Advanced Materials, University of Groningen, Nijenborgh 4, Groningen, AG 9747, Netherlands*

<sup>3</sup>*Departamento de Física, Universidade Federal de Pernambuco, 50670-901, Recife, Pernambuco, Brazil*

(Received 24 February 2021; revised 3 May 2021; accepted 1 July 2021; published 21 July 2021)

We report experiments on the control of intrinsic magnetic damping by thermal torque effects produced by the spin Seebeck effect and the anomalous Nernst effect in a thin layer of a ferromagnetic metal (Permalloy (Py), Ni<sub>81</sub>Fe<sub>19</sub>). Damping is measured in ferromagnetic resonance (FMR) experiments on a sample excited by microwave radiation and detected by the dc-voltage-generated spin rectification and magnonic charge pumping in the Py film. Application of a temperature gradient in the longitudinal configuration increases or decreases the dc-voltage line width, depending on the sign of the thermal gradient, demonstrating that the magnetic damping in Py is controlled by currents generated by thermal effects. The absolute values of the line-width changes in Py may reach 1 order of magnitude larger than in the ferrimagnetic insulator yttrium iron garnet. The large change in magnetic damping is interpreted as a superposition of different phenomena in the same metallic ferromagnet.

DOI: 10.1103/PhysRevApplied.16.014051

### I. INTRODUCTION

The continuing discoveries of processes to generate, transport, and detect spin currents are driving the field of spintronics to previously unforeseen possibilities [1–7]. The root of several spintronic phenomena in magnetic bilayers lies in the flow of spin angular momentum, with or without the flow of charge carriers, generated in a ferromagnetic material (FM) into an adjacent material or vice versa. However, some phenomena studied in the last decade were observed in a single ferromagnetic layer [8–12]. When a single ferromagnetic layer is excited by microwaves, the following effects stand out: spin rectification (SR) and magnetic charge pumping (MCP). SR represents the dc voltage due to nonlinear coupling between resistance and current caused by the magnetization dynamics [4,13–19]. On the other hand, MCP is the direct conversion of the spin current into charge current through the spin-orbit interaction. Such an effect represents magnetization precession into a ferromagnetic material with surface-inversion-symmetry breaking [9,11,20,21]. The SR and MCP phenomena associated with ferromagnetic resonance (FMR) can be studied simultaneously. These phenomena are intrinsic, mainly because they do not require a second material to convert spin current into a charge current or vice versa.

In fundamental terms, two phenomena stand out in the generation of spin-charge currents by a thermal gradient, namely, the spin Seebeck effect (SSE) and the anomalous Nernst effect (ANE). The spin Seebeck effect refers to the generation of a spin current by a thermal gradient in FMs. In the SSE, a temperature gradient,  $\nabla T$ , applied perpendicularly to the plane of the FM creates a spin current in the same direction. Such a spin current flows into an adjacent normal metal (NM), where it is converted, through the inverse spin Hall effect, into a charge current and detected by a pertinent dc voltage [22–24]. The electric field in the NM, expressed in terms of the thermal gradient applied perpendicularly to the plane, can be written in the form  $\vec{E}_{\text{SSE}} = -\alpha_S \hat{\sigma} \times \nabla T$ , where  $\alpha_S$  is often called the spin Seebeck coefficient, and  $\hat{\sigma}$  is the spin polarization in the direction of the applied magnetic field. In a bilayer made of a metallic FM film and a normal metal layer with a thermal gradient applied perpendicularly to the plane, one also expects to have a dc voltage due to the SSE [1,2]. Furthermore, in the single metallic FM film, there is also an electric field created by the ANE,  $\vec{E}_{\text{ANE}} = -\alpha_N \hat{\sigma} \times \nabla T$ , where  $\alpha_N$  is the anomalous Nernst coefficient [1–6,22–32]. In fact, in a single metallic FM film, the currents due to the SSE and ANE coexist, generating a superposition of both phenomena.

The flow of spin angular momentum with or without the flow of charge carriers allows the generation of a spin current that can produce a charge current. Thus, effects related to spin may be studied together with

\*joseholanda.papers@gmail.com and jose.silva.04@ufes.br

different processes in the same material. This relationship between different phenomena is promising for applications, for example, in heat-assisted magnetic recording, which is becoming increasingly important [33,34]. The SR, MCP, ANE, and SSE are usually studied experimentally with different setups and observed separately as well. Here, we study the control of magnetic damping by thermal effects in a single ferromagnetic Permalloy (Py, Ni<sub>81</sub>Fe<sub>19</sub>) layer with varying thickness. The magnetization dynamics is excited by microwave radiation in the FMR condition, resulting in a dc voltage due to SR and MCP. Control of magnetic damping is achieved by the currents due to the SSE and ANE. This finding represents an advance in the field of spin caloritronics in metallic FM films.

## II. EXPERIMENTAL SETUP

The Py samples are grown by dc sputtering on Si(0.4 mm)/SiO(300 nm), here simply called Si substrates, with a rectangular shape having lateral dimensions of 1.5 × 6 mm<sup>2</sup> and thicknesses,  $l_{\text{Py}}$ , varying from 5 to 100 nm. The typical pressures of base and argon are 10<sup>-8</sup> and 10<sup>-3</sup> Torr, respectively. The Py films have the same quality as in previous works [4,11]. For the dc-voltage measurements produced by the SR, MCP, SSE, and ANE phenomena, two silver strips 300 μm wide are deposited on the Py layer edges. In these strips, thin copper wires are attached with silver paint and connected to a nanovoltmeter to measure the dc voltage,  $V$ . The microwave signal used for the SR and MCP measurements is provided by a generator with frequency tunable over the range 5–8 GHz, with a fixed microwave power of  $P_S = 12$  mW on samples. Due to the low microwave power applied in our experiments, the microwave heating contributions [35,36] may be negligible. The microwave signal feeds a microstrip line with a characteristic impedance of 50 Ω made on a Duroid plate with a copper line 0.8 mm wide and a ground plane fixed in a copper support. The Py film placed on top of the

microstrip and separated by an 80-μm-thick Mylar sheet is excited by the rf magnetic field,  $h_{\text{rf}}$ , perpendicular to the magnetic field,  $H$ , applied in the film plane. The dc voltage,  $V$ , generated in the ferromagnetic resonance condition with fixed frequency is measured by sweeping the magnetic field for the complete series of single films.

For the application of a thermal gradient across the film, a commercial Peltier module, of width 2 mm, is used to heat or cool the side of the metallic layer, while the Si substrate is maintained in thermal contact with the copper microstrip and the Duroid plate. The temperature difference,  $\Delta T$ , across the Si/Py sample is calibrated as a function of the current in the Peltier module by means of a differential thermocouple, with one junction attached to a thin copper strip placed between the Peltier module and the sample structure and the other attached to the copper microstrip. After calibration, the thin copper strip and the thermocouple are removed, so as not to interfere with the dc voltage,  $V$ . Figure 1(a) shows the setup that allows the application of a microwave driving field and a temperature difference across the FM layer to measure the dc voltage,  $V$ . Figure 1(b) shows the resonance field versus frequency measured at several frequencies. The solid curve is obtained with the Kittel equation [37],  $f = \gamma[(H_R + H_A)(H_R + H_A + 4\pi M_{\text{eff}})]^{1/2}$ , where  $\gamma = 2.8$  GHz/kOe,  $4\pi M_{\text{eff}} = 4\pi M_S - H_S = 10.6$  kG, and anisotropy field  $H_A = 10$  Oe are values appropriate for Py obtained from the best fit, where  $M_S$  is the saturation magnetization,  $H_S = 2K_S/(M_S l_{\text{Py}})$ , and  $K_S$  is the surface anisotropy constant [38]. The agreement between the Kittel equation and data confirms that the voltage signals correspond to the FMR absorption.

## III. RESULTS AND DISCUSSION

Figures 2(a) and 2(c) show measurements of the dc voltage obtained with a microwave frequency of 7 GHz in two samples of a single layer of Py with thicknesses of

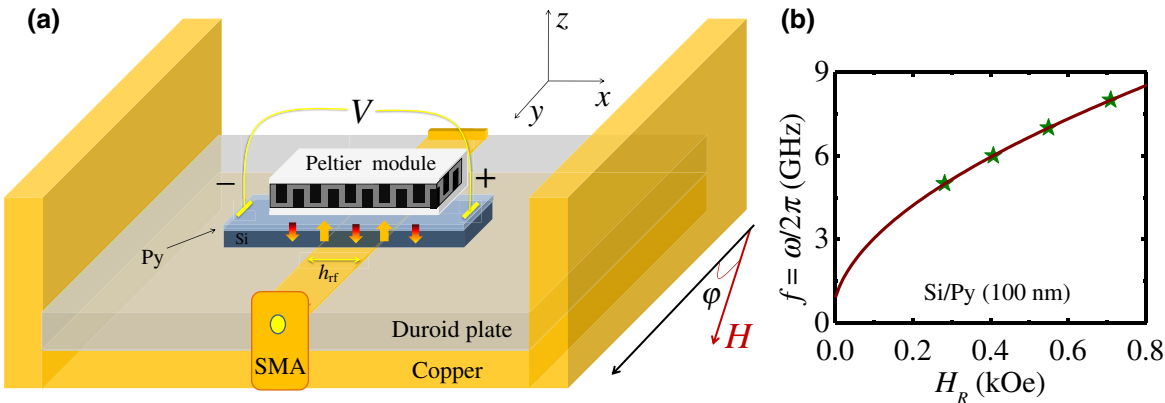


FIG. 1. (a) Sketch of the experimental setup and sample arrangement used for the simultaneous measurements of the SR, MCP, SSE, and ANE phenomena in Permalloy. Polarity of the measured voltages is indicated by plus and minus signs. (b) Symbols represent the measured resonance field as a function of the frequency, and the solid curve is obtained from the Kittel equation [37].

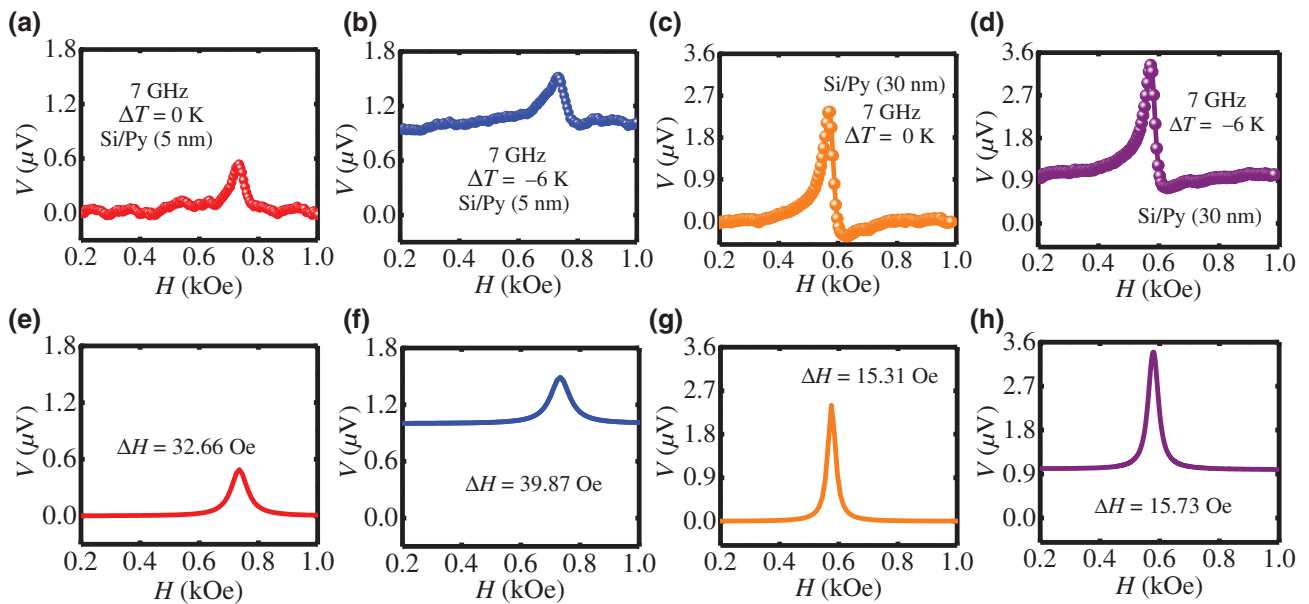


FIG. 2. Voltage,  $V$ , as a function of applied magnetic field measured in samples Si/Py (5 nm) and Si/Py (30 nm) at a frequency of 7 GHz with fixed power of  $P_S = 12$  mW. (a),(c) No temperature difference. (b),(d) With a temperature difference of  $\Delta T = -6$  K. (e)–(h) Symmetric components of lines in (a)–(d), respectively, showing line widths of  $\Delta H = 32.66$ ,  $39.87$ ,  $15.31$ , and  $15.73$  Oe.

5 and 30 nm and the magnetic field,  $H$ , applied along the  $y$  direction ( $\varphi = 0^\circ$ ), as defined in Fig. 1(a). The asymmetric line is typical of the SR and MCP effects in metallic FM films [11]. Figures 2(b) and 2(d) show similar measurements made with a temperature difference of  $\Delta T = -6$  K. To understand the behavior of the dc voltage generated in a single layer of Py under a thermal gradient, we investigate the line width obtained from the dc-voltage peaks. The field scanning voltages have an asymmetric line shape that can be fitted by a combination of symmetric Lorentzian and antisymmetric Lorentzian derivative functions given by [11]

$$V(H) = V_{\text{sym}} \frac{(\Delta H)^2}{[(H - H_R)^2 + (\Delta H)^2]} + V_{\text{asym}} \frac{\Delta H(H - H_R)}{[(H - H_R)^2 + (\Delta H)^2]}, \quad (1)$$

where  $V_{\text{sym}}$  and  $V_{\text{asym}}$  are the amplitudes of the symmetric and antisymmetric components, while  $\Delta H$  and  $H_R$  are the FMR line width and resonance field, respectively. With the fits from data in Figs. 2(a)–2(d) with Eq. (1), from the symmetric components in Figs. 2(e)–2(h) the following line widths are obtained: 32.66, 39.87, 15.31, and 15.73 Oe, respectively. These results show that the change in line width can be controlled by the thermal gradient and provide evidence of the Onsager reciprocity relationship between both phenomena, SSE and ANE, present in the metallic ferromagnetic. Similar to our previous work on yttrium iron garnet-platinum [39], the spin current that

flows parallel to the thermal gradient results in a change of the magnetic damping, measured via the line width of the voltage peak at the ferromagnetic resonance condition. However, in the case of Permalloy, the ANE adds up to the SSE for magnetic damping control. Such a contribution represents a relevant feature of the ANE, which is also observed in Heusler compounds [40–42].

Figure 3(a) shows the ANE and SSE charge currents, obtained by dividing the measured voltages by the resistances of the Py layers along the length of the Peltier element (2 mm), as a function of  $\Delta T$ , for  $H = \pm 0.9$  kOe and 7 GHz. In a metallic film such as Py, the application of a thermal gradient generates a voltage due to the ANE, but the spin current due to the SSE accumulates at the top of the Py film and below the natural oxide layer [9,11]. Therefore, with the application of microwave signals, the spin current due to the SSE is influenced by SR and MCP also being converted into charge current due to the Onsager reciprocity relationship in metallic ferromagnetic materials [4–7,9,11,43,44]. Figures 3(b)–3(f) show measurements of the field dependencies of the voltage,  $V$ , in the Py samples, produced by currents generated simultaneously by SR, MCP, SSE, and ANE, at frequencies of 5 and 7 GHz and a temperature difference of  $\Delta T = +6$  K, with the Si substrate cooler than the Py layer. Although the currents in the four processes (SR, MCP, SSE, and ANE) have different natures, they result in a single voltage that represents the superposition of all effects.

Figures 3(b)–3(f) also show that the contribution of the SR and MCP effects to the dc voltage as a function of the field, for several Py layer thicknesses, exhibits two

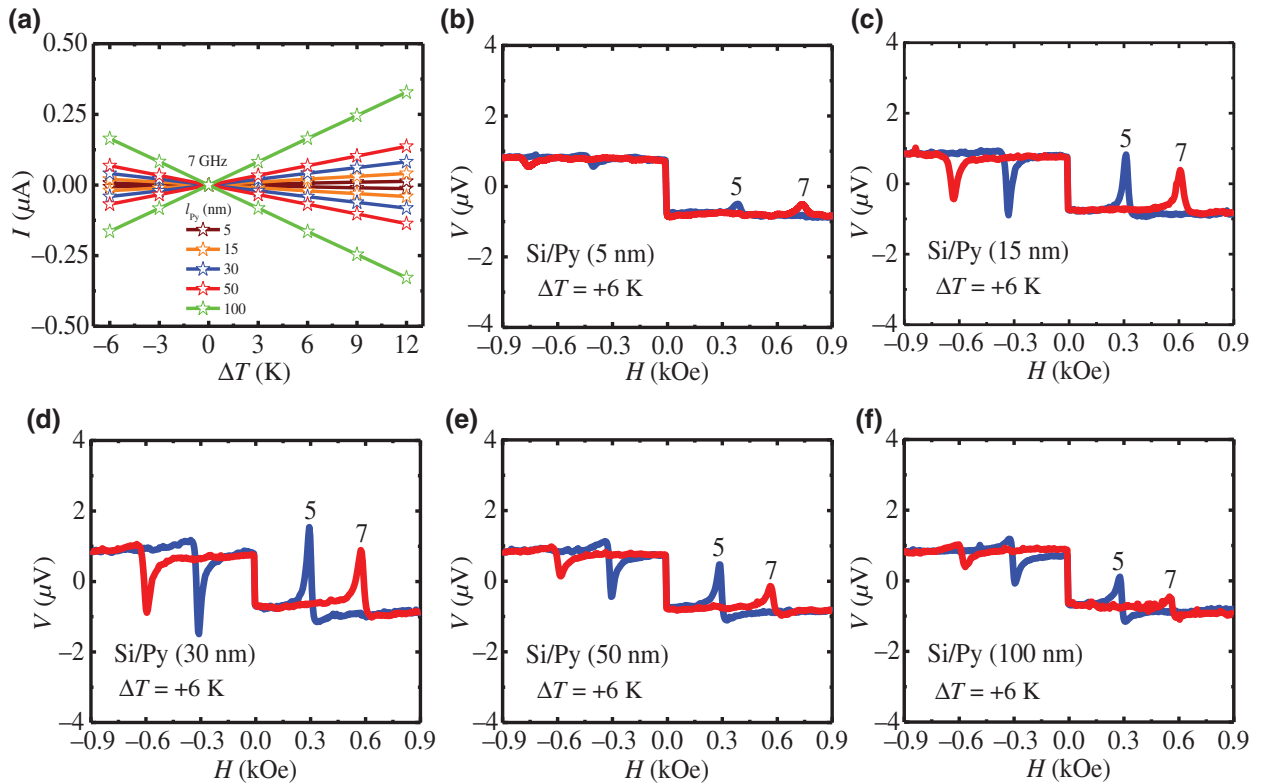


FIG. 3. (a) ANE and SSE charge currents, obtained by dividing measured voltages by resistances from the Py layers in the length of the Peltier element (2 mm) as a function of  $\Delta T$  for  $H = \pm 0.9$  kOe and 7 GHz. Here, there are ANE, SSE, SR, and MCP contributions. (b)–(f) Measurements of field dependencies of voltage  $V$  in the Py sample, produced by currents generated simultaneously by SR, MCP, SSE, and ANE, over frequencies from 5 and 7 GHz at a temperature difference of  $\Delta T = +6$  K.

different regimes. In the first regime, which corresponds to thicknesses ranging from 5 to 30 nm, the voltages increase with the thickness up to around 30 nm. This is the regime of thickness at which the surface perpendicular anisotropy field is operative and is responsible for the symmetry breaking normal to the films. In the second regime, which corresponds to thicknesses larger than 30 nm, the layers are thick enough, and the perpendicular anisotropy field does not play an important role anymore. In this case, the contribution of MCP is small compared with SR [9,11]. The SR and MCP effects are activated easily in Py films and controlled by the spin Hall effect [11,45,46], but there are no reports of control through thermal effects.

Figures 4(a)–4(e) show the variation of line widths with the temperature difference,  $\Delta T$ , measured for Py ( $l_{\text{Py}}$ ) at frequencies of 5, 6, 7, and 8 GHz. The line widths are measured by fitting of the measured line shapes with Eq. (1) as previously described. Even with the length of the Py film of 5 mm and nonuniform microwave excitation, only the uniform mode is excited, which is commonly obtained in Py [11–14,18,45–47].

The results in Figs. 4(a)–4(e) also show that magnetic damping abruptly decreases with a thickness up to 30 nm

and slowly increases with larger thicknesses, as shown in Fig. 4(f). Considering the magnetic damping parameter,  $\alpha = (\gamma/\omega)\Delta H$ , an essential role in the behavior of the dc-voltage line width can be given by  $\Delta H = \Delta H_0 + \Delta H_{2M} + \Delta H_{\text{eddy}}$ . Here,  $\Delta H_0$  is the value of the extrinsic contribution,  $\Delta H_{2M}$  is the two-magnon scattering contribution ( $\Delta H_{2M} = C_{2M}/l_{\text{Py}}^2$ ) [48], and the eddy-current contribution ( $\Delta H_{\text{eddy}} = C_{\text{eddy}}l_{\text{Py}}^2$ ) is important in the high-thickness regime [49]. The solid line shown in Fig. 4(f) is obtained with  $\Delta H_0 \approx 13$  Oe,  $C_{2M} = 395$  Oe  $\times$  nm<sup>2</sup>, and  $C_{\text{eddy}} = 2.2 \times 10^{-4}$  Oe/nm<sup>2</sup>, which is in good agreement with Refs. [9,11]. Notably, the absolute values of the line-width changes in Py shown in Fig. 4(a) is 1 order of magnitude larger than in the ferrimagnetic insulator yttrium iron garnet [3,6,36,50]. The proposal of control of magnetic damping is a most intriguing phenomenon associated with thermal effects and, in the experiments described here, a decrease in damping with increasing temperature gradient is visible in several ways. This means that simultaneous measurements allow control of the currents resulting from magnetization dynamic by thermal effects due to the Onsager reciprocity relationship between spin-charge currents.

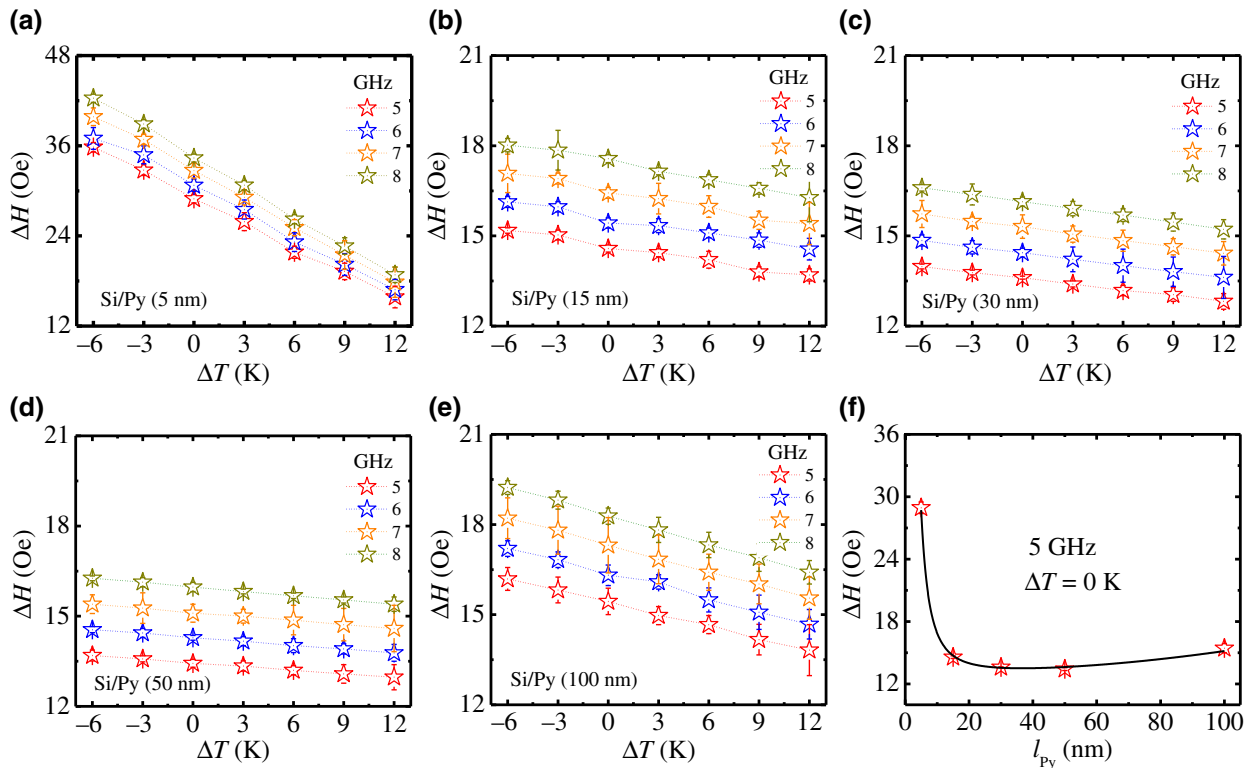


FIG. 4. (a)–(e) Line width as a function of temperature difference measured in Py with 5, 6, 7, and 8 GHz. (f) Dependence of line width as a function of thicknesses of Py films  $l_{\text{Py}}$ , for  $\Delta T = 0$  K and 5 GHz. Solid line is obtained with the expression for line width,  $\Delta H = \Delta H_0 + \Delta H_{2M} + \Delta H_{\text{eddy}}$ .

#### IV. CONCLUSIONS

The dc voltage,  $V$ , generated in single layers of Permalloy is measured under microwave-driven FMR conditions for a set of Permalloy films with thicknesses varying from 5 to 100 nm under an applied thermal gradient. All dc-voltage signals exhibit asymmetric line shapes that are a combination of symmetric Lorentzian and antisymmetric Lorentzian derivative curves. The dc-voltage measurements represent the voltage due to the superposition of the SR, MCP, SSE, and ANE effects. The dc-voltage line width shows that the magnetic damping in Py can be controlled by currents generated due to the thermal gradient. The damping increases or decreases depending on the sign of the thermal gradient. This behavior is reported for a single metallic ferromagnet and is much larger than that in insulating ferrimagnets. These findings represent a promising application of SSE and ANE phenomena in spin-caloritronic devices in electronics.

#### ACKNOWLEDGMENTS

This research is supported by the Conselho Nacional de Desenvolvimento Científico e Tecnológico (CNPq) and the Coordenação de Aperfeiçoamento de Pessoal de Nível Superior (CAPES) of Brazil.

- [1] K. Uchida, S. Takahashi, K. Harii, J. Ieda, W. Koshiba, K. Ando, S. Maekawa, and E. Saitoh, Observation of the spin Seebeck effect, *Nature* **455**, 778 (2008).
- [2] E. Padrón-Hernández, A. Azevedo, and S. M. Rezende, Amplification of Spin Waves by Thermal Spin-Transfer Torque, *Phys. Rev. Lett.* **107**, 197203 (2011).
- [3] L. Lu, Y. Sun, M. Jantz, and M. Wu, Control of FMR Relaxation in Thin Films Through Thermally Induced Interfacial Spin Transfer, *Phys. Rev. Lett.* **108**, 257202 (2012).
- [4] J. Holanda, O. Alves Santos, R. O. Cunha, J. B. S. Mendes, R. L. Rodríguez-Suárez, A. Azevedo, and S. M. Rezende, Longitudinal spin Seebeck effect in permalloy separated from the anomalous Nernst effect: Theory and experiment, *Phys. Rev. B* **95**, 214421 (2017).
- [5] S. M. Wu, W. Zhang, A. Kc, P. Borisov, J. E. Pearson, J. S. Jiang, D. Lederman, A. Hoffmann, and A. Bhattacharya, Antiferromagnetic Spin Seebeck Effect, *Phys. Rev. Lett.* **116**, 097204 (2016).
- [6] J. Holanda, D. S. Maior, O. Alves Santos, A. Azevedo, and S. M. Rezende, Evidence of phonon pumping by magnonic spin currents, *Appl. Phys. Lett.* **118**, 022409 (2021).
- [7] M. Kimata, H. Chen, K. Kondou, S. Sugimoto, P. K. Muduli, M. Ikhlas, Y. Omori, T. Tomita, A. H. MacDonald, S. Nakatsuji, and Y. Otani, Magnetic and magnetic inverse spin Hall effects in a non-collinear antiferromagnet, *Nature* **565**, 627 (2019).

- [8] R. Vidyasagar, O. Alves Santos, J. Holanda, R. O. Cunha, F. L. A. Machado, P. R. T. Ribeiro, A. R. Rodrigues, J. B. S. Mendes, A. Azevedo, and S. M. Rezende, Giant Zeeman shifts in the optical transitions of yttrium iron garnet thin films, *Appl. Phys. Lett.* **109**, 122402 (2016).
- [9] C. Ciccarelli, K. M. D. Hals, A. Irvine, V. Novak, Y. Tserkovnyak, H. Kurebayashi, A. Brataas, and A. Ferguson, Magnonic charge pumping via spin-orbit coupling, *Nat. Nanotech.* **10**, 50 (2015).
- [10] H. Saglam, C. Liu, Y. Li, J. Sklenar, J. Gibbons, D. Hong, V. Karakas, J. E. Pearson, O. Ozatay, W. Zhang, A. Bhattacharya, and A. Hoffmann, Anomalous Hall and Nernst Effects in FeRh, *arXiv:2012.14383* (28 Dec. 2020).
- [11] A. Azevedo, R. O. Cunha, F. Estrada, O. Alves Santos, J. B. S. Mendes, L. H. Vilela-Leão, R. L. Rodríguez-Suárez, and S. M. Rezende, Electrical detection of ferromagnetic resonance in single layers of permalloy: Evidence of magnonic charge pumping, *Phys. Rev. B* **92**, 024402 (2015).
- [12] E. Sagasta, Y. Omori, M. Isasa, Y. C. Otani, L. E. Hueso, and F. Casanova, Spin diffusion length of permalloy using spin absorption in lateral spin valves, *Appl. Phys. Lett.* **111**, 082407 (2017).
- [13] M. V. Costache, M. Sladkov, S. M. Watts, C. H. van der Wal, and B. J. van Wees, Electrical Detection of Spin Pumping due to the Precessing Magnetization of a Single Ferromagnet, *Phys. Rev. Lett.* **97**, 216603 (2006).
- [14] A. Azevedo, L. H. Vilela-Leão, R. L. Rodríguez-Suárez, A. F. Lacerda Santos, and S. M. Rezende, Spin pumping and anisotropic magnetoresistance voltages in magnetic bilayers: Theory and experiment, *Phys. Rev. B* **83**, 144402 (2011).
- [15] A. Yamaguchi, H. Miyajima, T. Ono, Y. Suzuki, and S. Yuasa, Rectification of radio frequency current in ferromagnetic nanowire, *Appl. Phys. Lett.* **90**, 182507 (2007).
- [16] L. H. Bai, Y. S. Gui, A. Wirthmann, E. Recksiedler, N. Mecking, C.-M. Hu, Z. H. Chen, and S. C. Shen, The rf magnetic-field vector detector based on the spin rectification effect, *Appl. Phys. Lett.* **92**, 032504 (2008).
- [17] S. Y. Huang, X. Fan, D. Qu, Y. P. Chen, W. G. Wang, J. Wu, T. Y. Chen, J. Q. Xiao, and C. L. Chien, Transport Magnetic Proximity Effects in Platinum, *Phys. Rev. Lett.* **109**, 107204 (2012).
- [18] H. Saglam, J. C. Rojas-Sánchez, S. Petit, M. Hehn, W. Zhang, J. E. Pearson, S. Mangin, and A. Hoffmann, Independence of spin-orbit torques from the exchange bias direction in Ni<sub>81</sub>Fe<sub>19</sub>/IrMn bilayers, *Phys. Rev. B* **98**, 094407 (2018).
- [19] A. Tsukahara, Y. Ando, Y. Kitamura, H. Emoto, E. Shikoh, M. P. Delmo, T. Shinjo, and M. Shiraishi, Self-induced inverse spin Hall effect in permalloy at room temperature, *Phys. Rev. B* **89**, 235317 (2014).
- [20] V. P. Amin, Junwen Li, M. D. Stiles, and P. M. Haney, Intrinsic spin currents in ferromagnets, *Phys. Rev. B* **99**, 220405(R) (2019).
- [21] A. Davidson, V. P. Amin, W. S. Aljuaid, P. M. Haney, and X. Fana, Perspectives of electrically generated spin currents in ferromagnetic materials, *Phys. Lett. A* **384**, 126228 (2020).
- [22] K. Uchida, H. Adachi, T. Ota, H. Nakayama, S. Maekawa, and E. Saitoh, Observation of longitudinal spin-Seebeck effect in magnetic insulators, *Appl. Phys. Lett.* **97**, 172505 (2010).
- [23] G. E. W. Bauer, E. Saitoh, and B. J. van Wees, Spin caloritronics, *Nat. Mater.* **11**, 391 (2012).
- [24] H. Adachi, K. Uchida, E. Saitoh, and S. Maekawa, Theory of the spin Seebeck effect, *Rep. Prog. Phys.* **76**, 036501 (2013).
- [25] J. Holanda, D. S. Maior, O. Alves Santos, L. H. Vilela-Leão, J. B. S. Mendes, A. Azevedo, R. L. Rodríguez-Suárez, and S. M. Rezende, Spin Seebeck effect in the anti-ferromagnet nickel oxide at room temperature, *Appl. Phys. Lett.* **111**, 172405 (2017).
- [26] S. Y. Huang, W. G. Wang, S. F. Lee, J. Kwo, and C. L. Chien, Intrinsic Spin-Dependent Thermal Transport, *Phys. Rev. Lett.* **107**, 216604 (2011).
- [27] A. D. Avery, M. R. Pufall, and B. L. Zink, Observation of the Planar Nernst Effect in Permalloy and Nickel Thin Films with in-Plane Thermal Gradients, *Phys. Rev. Lett.* **109**, 196602 (2012).
- [28] S. L. Yin, Q. Mao, Q. Y. Meng, D. Li, and H. W. Zhao, Hybrid anomalous and planar Nernst effect in permalloy thin films, *Phys. Rev. B* **88**, 064410 (2013).
- [29] D. Meier, D. Reinhardt, M. Schmid, C. H. Back, J.-M. Schmalhorst, T. Kuschel, and G. Reiss, Influence of heat flow directions on nernst effects in Py/Pt bilayers, *Phys. Rev. B* **88**, 184425 (2013).
- [30] B. F. Miao, S. Y. Huang, D. Qu, and C. L. Chien, Inverse Spin Hall Effect in a Ferromagnetic Metal, *Phys. Rev. Lett.* **111**, 066602 (2013).
- [31] C. Fang, C. H. Wan, Z. H. Yuan, L. Huang, X. Zhang, H. Wu, Q. T. Zhang, and X. F. Han, Scaling relation between anomalous nernst and Hall effect in [Pt/Co]<sub>n</sub> multilayers, *Phys. Rev. B* **93**, 054420 (2016).
- [32] Y.-J. Chen and S.-Y. Huang, Absence of the Thermal Hall Effect in Anomalous Nernst and Spin Seebeck Effects, *Phys. Rev. Lett.* **117**, 247201 (2016).
- [33] H. Z. Yang, Y. J. Chen, S. H. Leong, C. W. An, K. D. Ye, M. J. Yin, and J. F. Hu, A multifunctional test instrument for heat assisted magnetic recording media, *J. Appl. Phys.* **115**, 17B726 (2014).
- [34] J.-G. (Jimmy) Zhu and H. Li, Signal-to-noise ratio impact of grain-to-grain heating variation in heat assisted magnetic recording, *J. Appl. Phys.* **115**, 17B747 (2014).
- [35] F. L. Bakker, J. Flipse, A. Slachter, D. Wagenaar, and B. J. van Wees, Thermoelectric Detection of Ferromagnetic Resonance of a Nanoscale Ferromagnet, *Phys. Rev. Lett.* **108**, 167602 (2012).
- [36] M. B. Junglefleisch, T. An, K. Ando, Y. Kajiwara, K. Uchida, V. I. Vasyuchka, A. V. Chumak, A. A. Serga, E. Saitoh, and B. Hillebrands, Heat-induced damping modification in yttrium iron garnet/platinum hetero-structures, *Appl. Phys. Lett.* **102**, 062417 (2013).
- [37] S. M. Rezende, *Fundamentals of Magnonics, Lecture Notes in Physics* (Springer, Cham, 2020), Vol. 969.
- [38] B. Heinrich and J. F. Cochran, Ultrathin metallic magnetic films: Magnetic anisotropies and exchange interactions, *Adv. Phys.* **42**, 523 (1993).
- [39] J. Holanda, O. Alves Santos, R. L. Rodríguez-Suárez, A. Azevedo, and S. M. Rezende, Simultaneous spin pumping and spin Seebeck experiments with thermal control of

- the magnetic damping in bilayers of yttrium iron garnet and heavy metals: YIG/Pt and YIG/IrMn, *Phys. Rev. B* **95**, 134432 (2017).
- [40] M. Ikhlas, T. Tomita, T. Koretsune, M.-T. Suzuki, D. N. Hamane, R. Arita, Y. Otani, and S. Nakatsuji, Large anomalous Nernst effect at room temperature in a chiral antiferromagnet, *Nat. Phys.* **13**, 1085 (2017).
- [41] S. N. Guin, *et al.*, Anomalous Nernst effect beyond the magnetization scaling relation in the ferromagnetic Heusler compound Co<sub>2</sub>MnGa, *NPG Asia Mater.* **11**, 16 (2019).
- [42] X. Li, L. Xu, L. Ding, J. Wang, M. Shen, X. Lu, Z. Zhu, and K. Behnia, Anomalous Nernst and Righi-Leduc Effects in Mn<sub>3</sub>Sn: Berry Curvature and Entropy Flow, *Phys. Rev. Lett.* **119**, 056601 (2017).
- [43] Y. Tserkovnyak, A. Brataas, G. E. W. Bauer, and B. I. Halperin, Nonlocal magnetization dynamics in ferromagnetic heterostructures, *Rev. Mod. Phys.* **77**, 1375 (2005).
- [44] M. Weiler, H. Huebl, F. S. Goerg, F. D. Czeschka, R. Gross, and S. T. B. Goennenwein, Spin Pumping with Coherent Elastic Waves, *Phys. Rev. Lett.* **108**, 176601 (2012).
- [45] A. Hoffmann, Spin Hall effects in metals, *IEEE Trans. Magn.* **49**, 5172 (2013).
- [46] J. Holanda, H. Saglam, V. Karakas, Z. Zang, Y. Li, R. Divan, Y. Liu, O. Ozatay, V. Novosad, J. E. Pearson, and A. Hoffmann, Magnetic Damping Modulation in IrMn<sub>3</sub>/Ni<sub>80</sub>Fe<sub>20</sub> via the Magnetic Spin Hall Effect, *Phys. Rev. Lett.* **124**, 087204 (2020).
- [47] Y. Zhao, Q. Song, S.-H. Yang, T. Su, W. Yuan, S. S. P. Parkin, J. Shi, and W. Han, Experimental investigation of temperature-dependent gilbert damping in permalloy thin films, *Sci. Rep.* **6**, 22890 (2016).
- [48] A. Azevedo, A. B. Oliveira, F. M. de Aguiar, and S. M. Rezende, Extrinsic contributions to spin-wave damping and renormalization in thin Ni<sub>50</sub>Fe<sub>50</sub> films, *Phys. Rev. B* **62**, 5331 (2000).
- [49] B. Heinrich, R. Urban, and G. Woltersdorf, Magnetic relaxation in metallic films: Single and multilayer structures, *J. Appl. Phys.* **91**, 7523 (2002).
- [50] C. Hahn, G. de Loubens, O. Klein, M. Viret, V. V. Naletoev, and J. Ben Youssef, Comparative measurements of inverse spin Hall effects and magnetoresistance in YIG/Pt and YIG/Ta, *Phys. Rev. B* **87**, 174417 (2013).